International Geology Review, Vol. 46, 2004, p. XXX–XXX.

Experimental Faulting of Serpentinite During Dehydration: Implications for Earthquakes, Seismic Low-Velocity Zones, and Anomalous Hypocenter Distributions in Subduction Zones

HAEMYEONG JUNG[1] AND HARRY W. GREEN, II

Institute of Geophysics and Planetary Physics and Department of Earth Sciences, University of California, Riverside, California 92521

Abstract

Dehydration embrittlement of serpentine was investigated by employing triaxial deformation experiments at high pressure and temperature (P = 1–6 GPa; T = 550–820ºC). A modified Griggs apparatus was used up to 3.4 GPa and a Walker-type multi-anvil apparatus was used at 3.5–6 GPa). The investigated specimen is a serpentinized peridotite from Val Malenco, Italy. Dehydration of the sample under differential stress resulted in faults associated with ultrafine-grained solid reaction products, formed as byproducts of antigorite dehydration. This phenomenon was observed under all conditions tested (1–6 GPa, 630–820ºC), independent of pressure, even though the sign of total volume change (ΔV) of the dehydration reaction changes from positive to negative at 2.2 GPa. This observation confirms that dehydration embrittlement is a viable mechanism for triggering earthquakes independent of depth, so long as there is a hydrous mineral breaking down under differential stress. Aligned Mode-I cracks and fluid inclusion trails are common in relict olivines in the deformed serpentinite. We suggest that some of the puzzling observations, including a seismic low-velocity zone (LVZ) at the top of subducting slabs, can be attributable to aligned fluid-filled Mode-I cracks and enhanced defect mobility in olivine in the presence of water. The anomalous hypocenter distributions of earthquakes can be attributed to the degree of dehydration of hydrous minerals in combination with a certain level of stress. In addition, low-seismicity regions in subduction zones may be explained by "superplastic" flow under low stress along the ultrafine-grained solid reaction products that are produced during dehydration reactions.

Introduction

EARTHQUAKES OCCUR in subduction zones at depths down to ~ 680 km, even though faulting is inhibited at depth in the Earth due to high pressure and high temperature (Green and Houston, 1995; Kirby, 1995; Silver et al., 1995; Green and Marone, 2002). One popular hypothesis is that intermediate-depth earthquakes (~50–300 km) may be triggered by the dehydration embrittlement of serpentine or other hydrous minerals in subduction zones (Raleigh and Paterson, 1965; Raleigh, 1967; Murrell and Ismail, 1976; Rutter and Brodie, 1988; Mead and Jeonloz, 1991; Jiao et al., 2000; Peacock, 2001; Seno et al., 2001; Dobson et al., 2002; Hacker et al., 2003; Jung et al., 2004a; Mishra and Zhao, 2004; H. Zhang et al., 2004; Wang et al., 2004). However, a problem of this hypothesis is that fracture mechanics theory predicts that if the volume change (ΔV) resulting from a dehydration reaction becomes negative, there will be no shearing instability and therefore no faulting (Wong et al., 1997; Dobson et al., 2002). If this were true, it would be very difficult to explain intermediate-depth earthquakes, because at higher pressures the ΔV of reaction becomes negative in all systems likely to generate earthquakes. Previous deformation experiments were conducted only at low pressures (< 0.7 GPa), in which the total volume change (ΔV) is positive; experiments have not been performed previously at the higher pressures in the deep Earth where the total volume change is negative (e.g. at P > 2.2 GPa for antigorite; Ulmer and Trommsdorff, 1995).

Therefore, we investigated the mechanism of "dehydration embrittlement" over a wide range of pressures (1.0–6 GPa) and temperatures (630–820ºC) by deforming serpentinite under well-controlled physical conditions. We found that faulting was not inhibited when the volume difference between antigorite and its dehydration products

[1]Corresponding author; email: hjung@ucr.edu

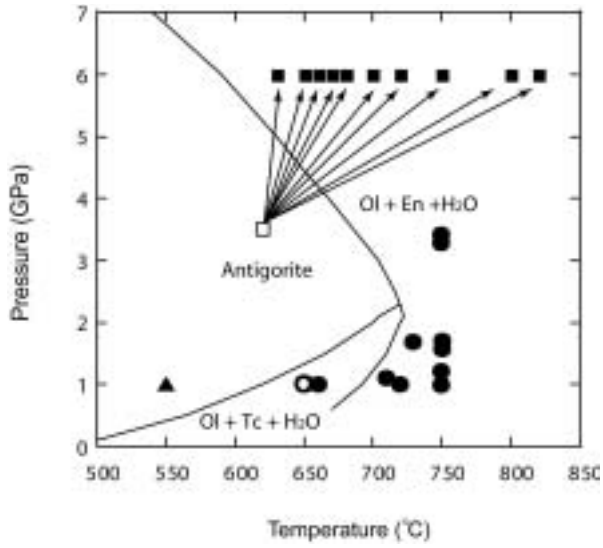

FIG. 1. Experimental conditions and phase diagram for antigorite. Phase boundaries are shown as solid lines (modified after Ulmer and Trommsdorff, 1995). Abbreviations: Ol = olivine; En = enstatite; Tc = talc. Open symbols indicate hydrostatic experiments (no faults produced). Deformation experiments using a modified Griggs apparatus (solid circles) with a strain rate $2 \times 10^{-4} s^{-1}$ showed faults and aligned dehydration products (Ol, Tc, En). Experiments in Walker-type multi-anvil apparatus (solid squares) generated stress by rapid pumping (arrows). In each experiment, the faulting could have happened at any place along the arrow (P-T run trajectory) after the arrow leaves the antigorite field. Fault-associated microstructures featuring aligned dehydration products were indistinguishable from those of samples deformed in Griggs apparatus. Filled triangle represents a deformation experiment without dehydration reaction, yielding a fault by brittle failure.

changed from positive to negative, showing that dehydration embrittlement is a viable mechanism to cause intermediate-depth earthquakes. A brief account of our study was reported in Jung et al. (2004a). We report here the details of experimental results on the deformation of a natural serpentinite, and discuss some implications for the generation of intermediate-depth earthquakes and the seismic LVZ at the top of subducting slabs, anomalous hypocenter distributions of earthquakes, and low-seismicity regions in subduction zones.

Experimental Procedures

The starting material for this work is a natural serpentinite from Val Malenco, Italy; the same material was used by Ulmer and Trommsdorff (1995) to determine the stability field of antigorite. The sample contains mostly antigorite, but also retains significant relict olivine and minor magnetite produced during serpentinization. We have chosen antigorite serpentinite because antigorite has the highest temperature and pressure stability field of serpentines and is likely the principal hydrous phase present in subducting mantle.

We used a modified Griggs apparatus; the sample assemblies used are similar to those illustrated in previous reports from our laboratory (Green and Borch, 1989; Burnley et al., 1991), with the additional modification of a furnace tapered at the bottom to minimize temperature gradients. Serpentinite cores (3.0 mm diameter and 8.4 mm long) were polished flat and square at both ends and encapsulated in Pt; oxygen fugacity was buffered by placing an Ni foil at both ends of the capsule. We used CsCl as a pressure medium to minimize friction between the specimen and piston and their surroundings.

In the later stages of this research, we used a new technique (Ni evaporation) to see clearly a fault offset after a deformation experiment. Ni was inserted as strain markers into our specimens as follows: The cored serpentinite was cut into disks ~ 200–500 μm long and Ni was evaporated on the top and bottom surfaces. For each experiment, 20–25 samples coated with Ni (~1 μm thick) were stacked inside a Pt capsule. To ensure that no deformation occurred

during pressurization, we used the following procedure: Pressure was increased first to 40 MPa and temperature was increased to 300ºC while pressure was kept at 40 MPa. When temperature reached 300ºC, pressure was increased to the designated pressure, and then temperature was increased to the target temperature. Samples were annealed for 0–60 minutes at the desired pressure and temperature before the deformation experiment was conducted. After deforming at a constant strain rate (2×10^{-4}/s), samples were quenched directly to room temperature in a few seconds. Pressure has an uncertainty of less than ~5% due to the variations during deformation. Pt/Rh (Type-B) thermocouples were placed at both the top and bottom of each sample; temperature uncertainty was less than ~10ºC as indicated by temperature differences recorded by the two thermocouples.

We also conducted experiments using a Walker-type multi-anvil at pressures of 3.5–6 GPa and temperatures of 630–820ºC. We used a graphite heater and W-3%Re/W-25%Re thermocouple. Specimens were 3.0 mm diameter and 7.0 mm long; alumina rods were placed at the top and bottom of the specimen to create nonhydrostatic stress during pressurization. The thermocouple junction was placed in the center of the specimen. Pressure was initially increased to 3.5 GPa, followed by increase of temperature to 620ºC in 1 hour. Both pressure and temperature were then increased simultaneously to the target pressure and temperature within 5–10 minutes in order to generate a strain rate approximately equivalent to the deformation experiments in the Griggs apparatus. By following the above procedures, we obtained fault microstructures similar to those produced in the Griggs apparatus.

After each experiment, the sample was examined by optical microscopy and scanning electron microscopy (SEM) employing XL-30 FEG at the University of California in Riverside. Backscattered electron images (BEI) were taken at 20 kV acceleration voltage and 10 mm working distance for the starting material as well as the deformed samples. Mineral phases of the starting materials and dehydration products of antigorite were analyzed using energy-dispersive spectroscopy (EDS) in the SEM.

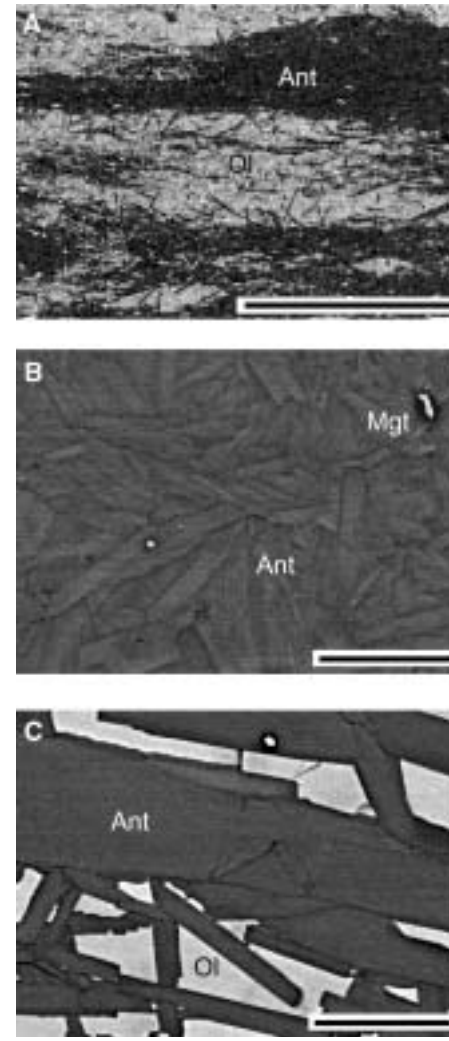

FIG. 2. Backscattered electron images of the starting material (serpentinized peridotite). A. Low-magnification image. Abbreviations: Ant = antigorite; Ol = olivine. B. Magnified view of an antigorite-rich area. The small bright area is magnetite (Mgt). C. Magnified view of relict olivine partially replaced by antigorite, showing straight phase boundaries between olivine and antigorite and lack of fluid inclusion trails in olivine. Scale bars: 1 mm (A); 20 µm (B, C).

Results

Experimental conditions and results are summarized in Figure 1 (modified after Jung et al., 2004a) and Table 1. Typical microstructures of the starting material (serpentinized peridotite) are shown in Figure 2. Only in rare cases does relict olivine in the starting material show fluid inclusion trails (Fig. 2C). Grain boundaries between the relict olivine and antigorite are extremely straight. Minor magnetite is also present.

TABLE 1. Experimental Conditions and Results

Run no.[1]	P, GPa	T, °C	Annealed time before deformation, min	Strain rate, 1/s	Results and comments
GL714	1.0	660	60	2×10^{-4}	Faulted
GL715	1.0	650	60	–	No faults, no deformation
GL716	1.2	750	60	2×10^{-4}	Faulted
GL717	1.0	550	60	2×10^{-4}	Faulted[3]
GL718	1.7	750	60	2×10^{-4}	Faulted
GL723	1.6	750	60	2×10^{-4}	Faulted
GL725	1.0	750	60	2×10^{-4}	Faulted
GL726	1.0	720	0	2×10^{-4}	Faulted
GL727	1.7	730	0	2×10^{-4}	Faulted
GL728	1.1	710	0	2×10^{-4}	Faulted
GB290	3.4	750	60	2×10^{-4}	Faulted
GB292	3.3	750	20	2×10^{-4}	Faulted
M501	6	680	–	–	Faulted microstructures[4]
M502	3.5	620	–	–	No faults, no deformation
M504	6	670	–	–	Faulted microstructures[4]
M505	6	660	–	–	Faulted microstructures[4]
M506	6	650	–	–	Faulted microstructures[4]
M507	6	630	–	–	Faulted microstructures[4]
Ma164[2]	6	700	–	–	Faulted microstructures[4]
Ma167[2]	6	750	–	–	Faulted microstructures[4]
Ma172[2]	6	800	–	–	Faulted microstructures[4]
Ma173[2]	6	720	–	–	Faulted microstructures[4]
Ma179[2]	6	820	–	–	Faulted microstructures[4]

[1]Runs of GL- and GB-series experiments are from Griggs apparatus; runs of M- and Ma-series experiments are from Walker-type multi-anvil apparatus.
[2] Data from Jung et al., 2004a.
[3] Faulted by conventional brittle failure without dehydration (see details in text and in Fig. 1).
[4] Fault-associated microstructures are similar to those of samples deformed in Griggs apparatus.

Sample GL 715 (open circle in Fig. 1) was pressurized to 1.0 GPa and annealed for 1 hour at 650ºC (e.g., see Table 1). The sample was quenched without deformation to see the effect of pressurization and annealing on the sample. The sharp corners on the specimen and the complete lack of deformation of the Pt capsule shows that our pressurization procedure allows successful arrival at pressure without introducing deformation in the specimen (Fig. 3) and that dehydration of serpentine itself does not cause faulting. Sample GL715 showed evidence of dehydration of antigorite (e.g., irregular grain boundaries against relict olivine due to the nucleation of small amounts of olivine and talc, and fluid inclusion trails in relict olivine, Fig. 3B).

Faults were generated under stress by deforming samples at high pressure and temperature. One specimen was deformed within the antigorite stability field (GL 717, shown as a filled triangle in Fig. 1). This sample failed by conventional brittle

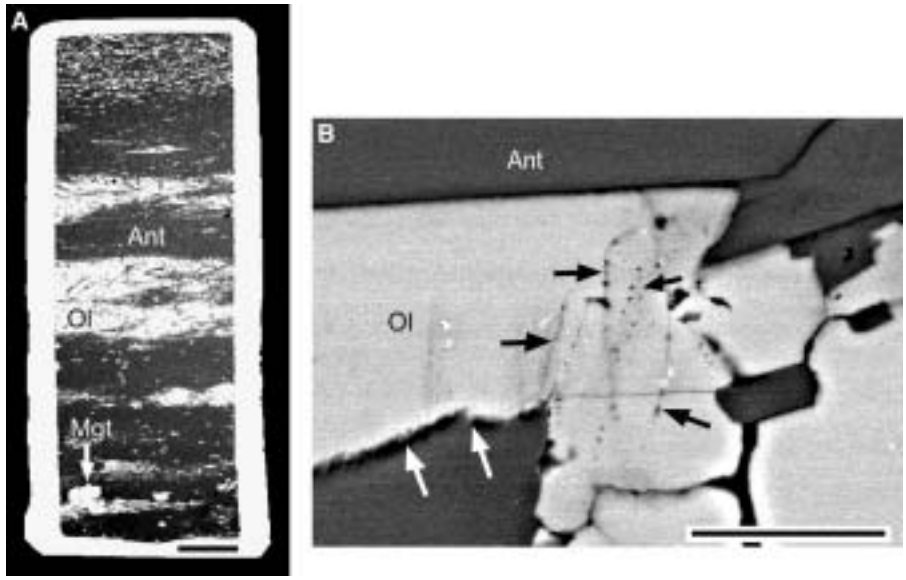

FIG. 3. Backscattered electron images of sample (open circle in Fig. 1) pressurized to 1.0 GPa and annealed for 1 hour at 650ºC. A. Platinum capsule (white). Other legends are the same as in Figure 2. Both specimen and Pt capsule undeformed. No faulting was generated. B. Detail of (A), showing evidence of dehydration of antigorite such as irregular, open, grain boundaries (white arrows) and fluid inclusion trails (black arrows) in relict olivine. Scale bars: 1 mm (A); 10 μm (B).

fracture under a very high differential stress (1.5 GPa) and showed no evidence of dehydration of antigorite. All other samples were deformed outside the antigorite stability field (Fig. 1) and displayed faults associated with ultrafine-grained solid dehydration products (Figs. 4–6). The dehydration products are olivine plus talc or enstatite (with grain size = 300 nm). Faults are aligned at ~30 ± 15º to the maximum principal stress orientation. Fault offset is clearly shown by offset of natural features and by our technique of evaporating Ni onto disks of sample and stacking them (Figs. 4A and 5). It is also notable that evidence for dehydration reaction is very much less distant from fault zones, strongly suggesting that reaction started in a narrow zone under stress and propagated to establish the faults (Figs. 4–6). Samples faulted by dehydration embrittlement showed the following characteristics: (1) many fluid inclusion trails in Mode-I orientation are observed inside relict olivine (Fig. 7); (2) Mode-I cracks are common in relict olivine (Figs. 4B, 4D, 5A, and 7); (3) grain boundaries between olivine and antigorite, and cracks in olivine show evidence of dissolution in the presence of water and displayed irregular cuspate shapes (Fig. 8). These observations indicate that the fluid (H_2O) produced by the dehydration reaction was mobile and initially unsaturated in olivine components.

Typical microstructures of the initial stages of faults are shown in Figure 6. Figure 6A shows a fault trace at P = 1.0 GPa that displays wispy-solid reaction products (light grey features pointed out by arrowheads) aligned approximately normal to the macroscopic maximum prinicipal stress, σ_1 (N-S), defining surfaces similar to stylolites (Rispoli, 1981) or anticracks (Flecher and Pollard, 1981), surfaces across which contraction has occurred and volume has been lost. Branching of the left-lateral fault is seen at the top right corner of the image, with compression (anticrack) lenses in the squeezed wedge (arrow). A very common observation in our experiments at all pressures are *en echelon* fault segments aligned such that the region between them experienced compression. These "push-togethers" are so defined to identify their analogy to "pull-aparts" commonly observed in the field and in experiments, when the alignment of *en echelon* fault segments is such that the region between them experienced extension. Figure 6B shows a series of such "push-togethers" (arrowheads) at P = 6 GPa. Note that the

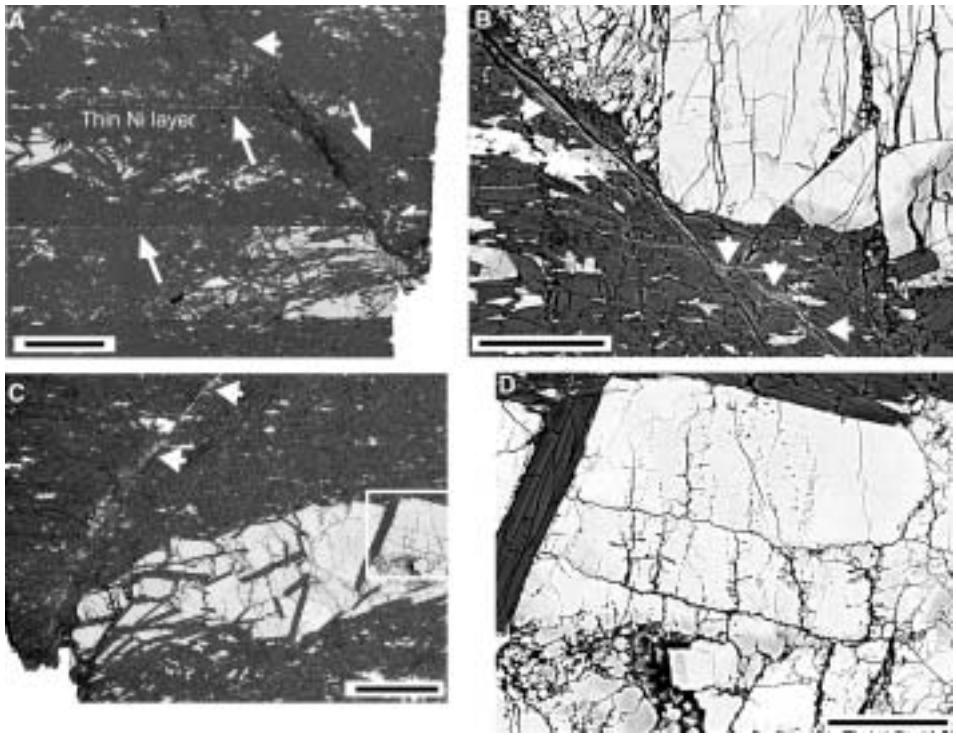

FIG. 4. Backscattered electron images of faulted samples. White arrowheads indicate solid dehydration products. A. Sample deformed at 1.0 GPa and 720ºC at a constant strain rate of 2×10^{-4} s^{-1} ($\Delta V > 0$). A fault offset is clearly visible by displacement of Ni films evaporated on disks of serpentinite stacked as sample (white arrows). B. Magnified view of different area of same sample showing abundant Mode-I cracks in relict olivine and dehydration products along fault zones. C. Sample deformed at 3.3 GPa, 750ºC, 2×10^{-4} s^{-1} ($\Delta V < 0$). Fault offset shown by displacement of specimen/Pt interface; aligned dehydration products along fault are indicated by arrowheads. D. Detail of the right side of panel (C), showing many Mode-I cracks and fluid inclusions trails inside relict olivine. Scale bars: 200 μm (A, C); 50 μm (B, D).

abundance of anticrack lenses is greater in these regions, where they function to accommodate the shortening imposed by the local stresses between the fault segments (see also Jung et al., 2004a).

In summary, fault zones in all of our specimens are characterized by fine-grained solid dehydration products along their length and in anticrack lenses adjacent to them. *En echelon* fault segments are very common, with stepping always such that compressive stresses were generated by fault displacements and were accommodated by anticrack lenses of the solid dehydration products (Figs. 4, 6, and 9). No microstructural differences were observed between faults generated at low pressures (1.0–1.7 GPa), where the volume change of reaction (ΔV) was positive, and those observed at higher pressures (3.3–6 GPa) where the volume change of reaction (ΔV) was negative.

Discussion and Geophysical Implications

The persistence of faulting at all pressures investigated (Figs. 4, 6, and 9), regardless of the sign of the volume change (ΔV) during the dehydration reaction is contrary to the prediction by conventional rock mechanics theory of pore-pressure-aided faulting (Wong et al., 1997; Dobson et al., 2002). We believe that the resolution of this conundrum is that, under stress, the fluid and solid reaction products separate as they are being generated, or very shortly thereafter. As such, the ΔV of both types of reaction products can participate in triggering the faulting instability; the fluid ($\Delta V_f > 0$) functions in the normal way by assisting opening of Mode-I microcracks and the solid reaction products ($\Delta V_s < 0$) function by "opening" Mode-I microanticracks, analogous to faulting during the olivine $\rightarrow$ spinel transformation

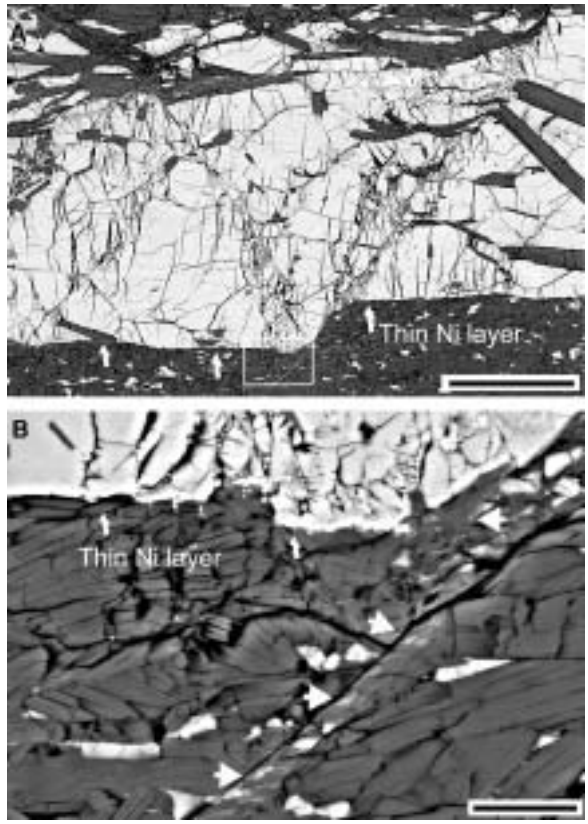

FIG. 5. Backscattered electron images showing abundant Mode-I cracks. A. Sample deformed at 1.1 GPa and 710ºC. Several faults propagated through the olivine rich layer ~200 µm thick; the largest has a fault offset of ~50 µm, shown by the thin Ni-evaporation (white arrows). B. Magnified view of the inset in (A) showing Ni layer (white arrows) and dehydration products (arrow heads) along the fault. Scale bars: 100 µm (A); 10 µm (B).

(Green and Burnley, 1989; Green et al., 1990; Burnley et al., 1991). Our observations on antigorite faulting (see also Jung et al., 2004a) clearly show that such separation of fluid and solid dehydration products occurs during or immediately after dehydration under stress. Whether this interpretation is correct or not, the experimental observations demonstrate that dehydration embrittlement is a viable mechanism for triggering earthquakes independent of depth, so long as there is a mineral dehydrating under differential stress.

Recent seismic data suggest that a seismic low-velocity zone (LVZ) approximately 1–7 km thick is a persistent feature of many subduction zones including Alaska, the Aleutians, the Kuriles, the Marianas, northern Japan, and Nicaragua (Abers, 2000; Abers et al., 2003; Ferris et al., 2003; Mishra and Zhao, 2004). Ferris et al. (2003) showed that the LVZ is even 11–22 km thick in central Alaska. The LVZs exist at the top of the subducting slabs at depths of ~50–250 km, with both P- and S-wave velocities consistently ~5–7% lower than the surroundings. We propose here that this seismic LVZ may be attributed to the accumulation of Mode-I cracks under stress and enhanced defect mobility during and/or after dehydration of hydrous minerals. The reduction of seismic velocity can be caused by the existence of open cracks (Anderson et al., 1974; Paterson, 1978). Figures 4, 5, and 7 show many aligned Mode-I cracks nearly parallel to the maximum principal stress orientation which were formed in response to dehydration of serpentine under stress. These aligned cracks are commonly observed in the deformed samples, and can reduce seismic velocities at the top of the subducting slabs. Similar Mode-I microcracks and faulting are also observed

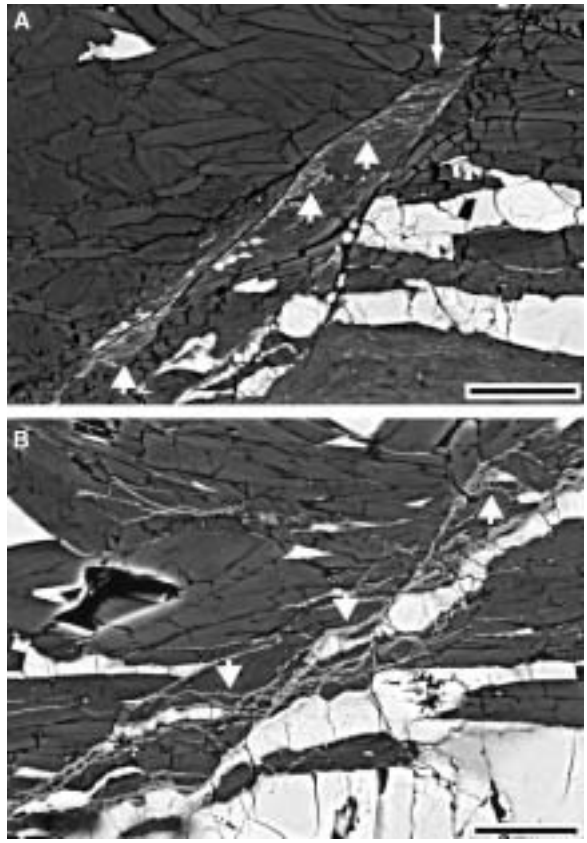

FIG. 6. Maximum compression direction is N-S in images. Backscattered electron images of fault microstructures. A. Sample deformed at 1.0 GPa and 650ºC ($\Delta V > 0$). Convergence zone (arrow) is under compression and exhibits a concentration of solid dehydration products (grey "wisps") oriented normal to the orientation of σ_1. The multiple "wisps" are anticracks recording volume loss in the compressed zone (arrowheads) (see also Jung et al., 2004a). B. Similar microstructures from a multi-anvil sample faulted at 6 GPa and 750ºC ($\Delta V < 0$), showing similar anticrack lenses in a series of "push togethers" (arrowheads) between *en echelon* fault segments at high pressure (see text for discussion). Scale bars: 20 μm.

in deformed eclogite (J. Zhang et al., 2004), which could give the same effects of lowering seismic velocities. The reduction of seismic velocity could also be caused by enhanced defect mobility in relict olivine due to the presence of dissolved water (through anelastic relaxation; Karato, 1995). Previous experimental studies showed that the mobilities of defects in olivine including point defects, dislocations, and grain boundaries are enhanced by the presence of a small amount of water (Mackwell et al., 1985; Karato et al., 1986; Mei and Kohlstedt, 2000; Jung and Karato, 2001a, 2001b; Karato and Jung, 2003). This effect of water on the reduction of seismic velocity will be much more significant at high pressures because a significant amount of water can be soluble in olivine at high pressures (Kohlstedt et al., 1996; Jung et al., 2004b).

The hypocenter distributions of earthquakes in Alaska (Ferris et al., 2003) coincide with the location of the seismic LVZs at the top of the subducting slab. This phenomenon might be explained by the dehydration of a hydrous mineral under stress in the subducting slab. As shown in this study, the initiation site of a fault (e.g. hypocenter of an earthquake) by dehydration embrittlement of serpentine (Fig. 5) can be coincident with the seismic LVZs.

Recent studies of seismic tomography and magnetotelluric surveys suggest the existence of fluids at

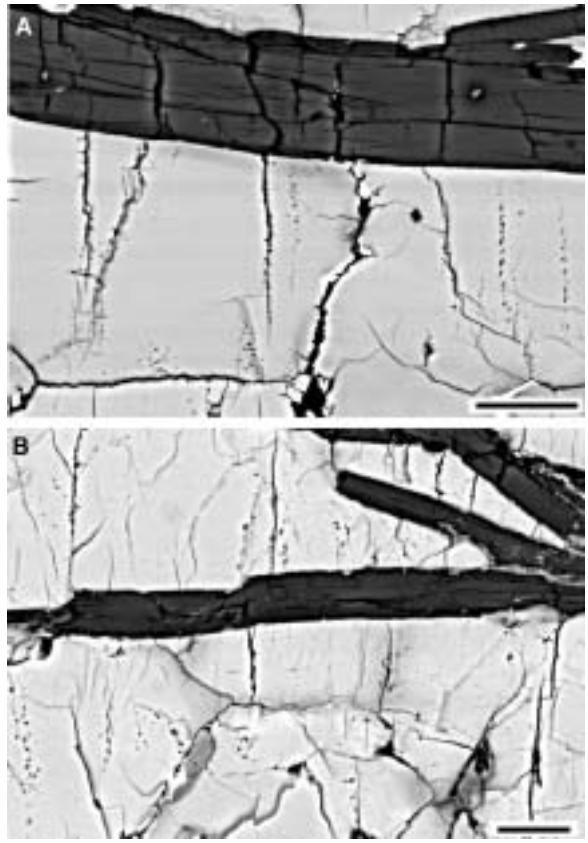

FIG. 7. Backscattered electron images showing Mode-I cracks and fluid inclusion trails in relict olivine. A. Sample deformed at 1.7 GPa and 730ºC ($\Delta V > 0$) in Griggs apparatus. B. Sample deformed in multi-anvil to 6 GPa and 750ºC ($\Delta V < 0$) showing similar Mode-I cracks and fluid inclusion trails. Maximum compression direction is N-S in images. Scale bars: 20 μm.

the hypocenter of the disastrous 1995 Kobe earthquake (Mw 7.2) in Japan (Zhao et al., 1996, 2002; Salah and Zhao, 2003), the catastrophic 2001 Bhuj earthquake (Mw 7.6) in India (Kayal et al., 2002), and at least some earthquakes along the San Andreas fault in California (Unsworth et al., 1997; Bedroisan et al., 2002). These earthquakes are characterized by low seismic S-wave velocity and high Poisson's ratio and/or low resistivity, indicating that the anomaly may be due to fluid-filled rocks. The fluid might have contributed to the initiation of the earthquakes, which is consistent with our experimental observations in this study. A potential source of fluids is dehydration of hydrous minerals (e.g. serpentine).

Hypocenter distributions of earthquakes for both main shocks and aftershocks were reported in several recent studies (Unsworth et al., 1997; Bedroisan et al., 2002; Kayal et al., 2002; Zhao et al., 2002, 2004; Salah and Zhao, 2003) and appear to be anomalous, as described below. The observed hypocenters are distributed between the highest and the lowest Vs velocity, between the highest and lowest Poisson's ratio, and between the highest and lowest resistivity. This phenomenon is consistent with the presence of water in the study area. We propose that there may be a certain critical stress under which seismicity occurs in combination with the presence of water along the aligned dehydration products (Fig. 9) or in the pre-existing fault zone. The region of the highest Vs, the lowest Poisson's ratio, and the highest resistivity may have no water present because of an absence of dehydration, showing an absence of seismicity. In contrast, the region of

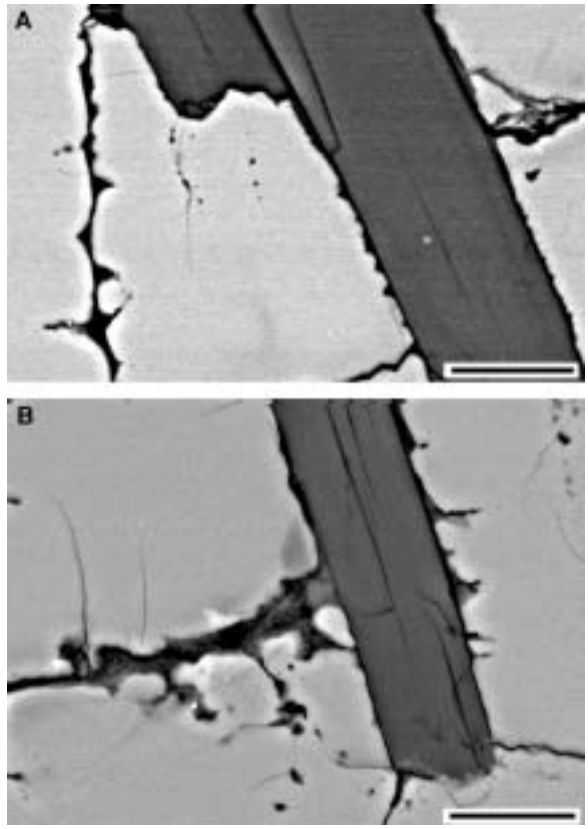

FIG. 8. Backscattered electron images showing dissolution along boundaries within olivine and between olivine and antigorite after dehydration reaction in the sample. A. Sample deformed at 1.7 GPa and 750ºC ($\Delta V > 0$). B. Sample deformed 3.3 GPa and 750ºC ($\Delta V < 0$). Scale bars: 10 μm.

the lowest Vs, the highest Poisson's ratio, and the lowest resistivity may have too much water (too much dehydration of a mineral) to allow seismicity to be triggered. If there is too much water present along either the aligned dehydration products or a pre-existing fault by the dehydration of hydrous minerals, rather than inducing faulting, the aligned dehydration products within a pre-existing fault zone could result in greatly increased grain-boundary sliding and rolling (Shan et al., 2004) resulting in "superplastic" flow under a low stress (Fig. 9), yielding an absence of seismicity. This could be due to the existence of ultrafine-grained dehydration products, allowing efficient grain boundary sliding (Fig. 9D). The existence of partial melt (Jin et al., 1994; Jung and Waff, 1998; Zimmerman et al., 1999; J. Zhang et al., 2004) may also cause a similar effect. If there is enough partial melt to be connected, the fault zone may be expected to be lubricated without causing seismicity.

Recently, scientists have been puzzled by observations of a distinct low-seismicity zone and even aseismic zone in some of the presumed serpentinized mantle wedges, such as above the subducting lithosphere under Japan (Kasahara et al., 2001; Fujie et al., 2002; Obara, 2002; Ozawa et al., 2002, 2004; Kodaira et al., 2004) and Casdadia (Dragert et al., 2001; Brocher et al., 2003; Rogers and Dragert, 2003). Such behavior also could perhaps be explained by "superplastic" flow under low stress along ultrafine-grained dehydration products, with or without the presence of fluid (Fig. 9).

Possible mechanisms of the hydration of a subducting slab that were previously reported are penetration of seawater into the oceanic mantle via a transform fault (Francis, 1981), high-temperature

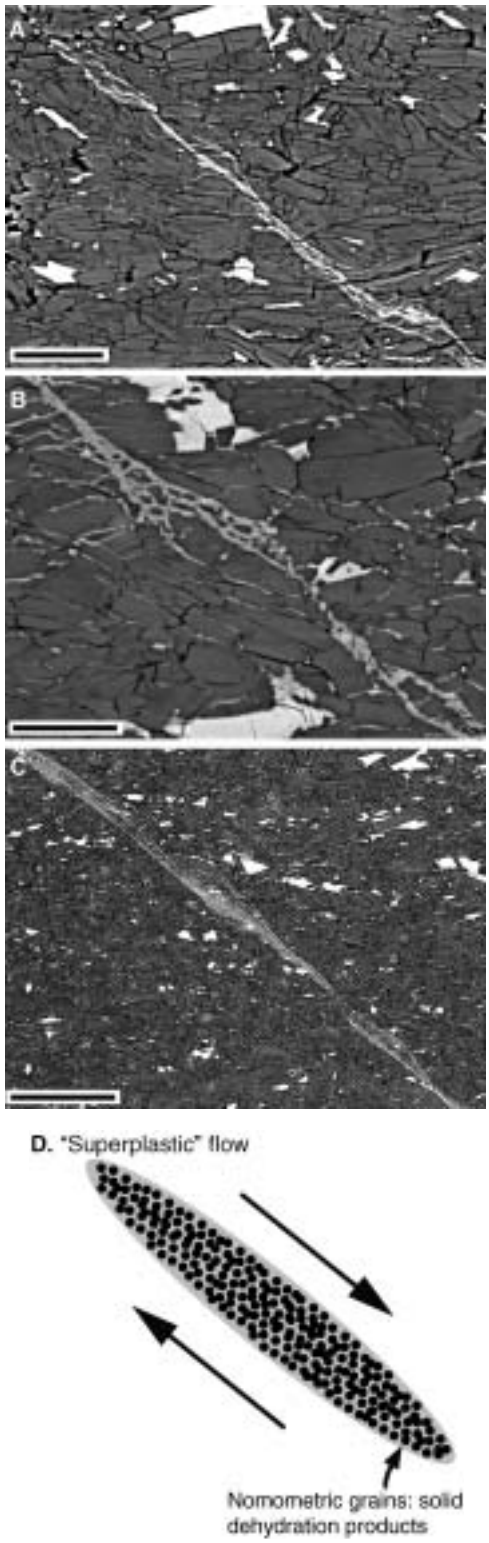

FIG. 9. Backscattered electron images showing aligned dehydration products at three pressures. The aligned solid dehydration products are formed in a localized zone. A. Sample deformed at 1.7 GPa, 750ºC ($\Delta V > 0$). B. Sample deformed at 3.3 GPa, 750ºC ($\Delta V < 0$). C. Sample deformed at 6.0 GPa, 630ºC ($\Delta V < 0$). D. Schematic drawing illustrating potential "superplastic" flow along solid dehydration products. Scale bars: 20 μm (A, B); 100 μm (C).

alteration of ultramafics in the upper mantle beneath a fracture zone (Kimball et al., 1985), and deep seawater injection along a major fault in a subducting plate ruptured by a trench–outer rise event (Peacock, 2001). A summary of the evidence for serpentinization of the oceanic lithosphere was also reported by Escartin et al. (1997). Omori et al. (2002) estimated that the maximum degree of serpentinization in a N-S cross-section of the Kanto area in Japan reached ~50 vol%, involving a substantial serpentinization of the peridotite down to ~100 km. Active serpentine mud volcanoes in the Mariana forearc (Fryer, 1996) and serpentinite seamounts in the Izu-Bonin and Mariana forearc regions (Fryer, 1996; Maekawa et al., 2001) provide additional supporting evidence for the existence of a serpentinized mantle wedge.

Summary and Concluding Remarks

Deformation of a naturally serpentinized peridotite resulted in faults by dehydration embrittlement of serpentine under all conditions tested (1–6 GPa, 630–820ºC), showing that dehydration embrittlement is a viable mechanism to cause intermediate-depth earthquakes, regardless of the sign of total volume change of reaction. The seismic LVZ at the top of the subducting slabs could be attributable to aligned Mode-I cracks and the enhanced defect mobility in the presence of water, which come from the dehydration of hydrous minerals. The anomalous hypocenter distributions of earthquakes may be attributable to the degree of dehydration of hydrous minerals in combination with a certain level of stress. Distinct low-sesmicity zones could also be explained by "superplastic" flow under low stress along the ultrafine-grained dehydration products, with or without the presence of a fluid.

Acknowlegments

HWG thanks Bob Coleman for many years of inspiration in the study of ophiolites and other

related mantle rocks. Very fond memories remain of the 1973 Ophiolite Field Conference traveling through Oregon and California. Thanks for the memories, Bob! We thank V. Trommsdorff for sample material corresponding to that used in Ulmer and Trommsdorff (1995). G. A. Abers, P. G. Silver, and L. F. Dobrzhinetskaya provided helpful discussions. We are grateful to J. Zhang and E. Riggs for constructive reviews. F. Forgit provided expert specimen assembly preparation and laboratory assistance. This work was supported by the US National Science Foundation grants #EAR0125938 and #EAR0135411.

REFERENCES

Abers, G. A., 2000, Hydrated subducted crust at 100–250 km depth: Earth and Planetary Science Letters, v. 176, p. 323–330.

Abers, G. A., Plank, T., and Hacker, B. R., 2003, The wet Nicaraguan slab: Geophysical Research Letters, v. 30, no. 2, p. 1098 [doi:10.1029/2002GL015649].

Anderson, D. L., Minster, B., and Cole, D., 1974, The effect of oriented cracks on seismic velocities: Journal of Geophysical Research, v. 79, p. 4011–4015.

Bedroisan, P. A., Unsworth, M. J., and Egbert, G., 2002, Magnetotelluric imaging of the creeping segment of the San Andreas fault near Hollister: Geophysical Research Letters, v. 29, no. 11 [doi: 10.1029/2001GL014119].

Brocher, T. M., Parsons, T., Tréhu, A. M., Snelson, C. M., and Fisher, M. A., 2003, Seismic evidence for widespread serpentinized forearc upper mantle along the Cascadia margin: Geology, v. 31, p. 267–270.

Burnley, P. C., Green, H. W., and Prior, D. J., 1991, Faulting associated with the olivine to spinel transformation in Mg_2GeO_4 and its implications for deep-focus earthquakes" Journal of Geophysical Research, v. 96, p. 425–443.

Dobson, D. P., Meredith, P. G., and Boon, S. A., 2002, Simulation of subduction zone seismicity by dehydration of serpentine: Science, v. 298, p. 1407–1410.

Dragert, H., Wang, K. and James, T. S., 2001, A silent slip event on the deeper Cascadia subduction interface: Science, v. 292, p. 1525–1528.

Escartín, J., Hirth, G., and Evans, B., 1997, Nondilatant brittle deformation of serpentinites: Implications for Mohr-Coulomb theory and the strength of faults: Journal of Geophysical Research, v. 102, p. 2897–2913.

Ferris, A., Abers, G. A., Christensen, D. H., and Veenstra, E., 2003, High resolution image of the subducted Pacific (?) plate beneath central Alaska, 50–150 km depth: Earth and Planetary Science Letters, v. 214, p. 575–588.

Fletcher, R. C., and Pollard, D. D., 1981, Anticrack model for pressure solution surfaces: Geology, v. 9, p. 419–424.

Francis, T. J. G., 1981, Serpentinization faults and their role in the tectonics of slow spreading ridges: Journal of Geophysical Research, v. 86, p. 11616–11622.

Fryer, P., 1996, Tectonic evolution of the Mariana convergent margin: Review of Geophysics, v. 34, p. 89–125.

Fujie, G., Kasahara, J., Hino, R., Sato, T., Shinohara, M., and Suyehiro, K., 2002, A significant relation between seismic activities and reflection intensities in the Japan Trench region: Geophysical Research Letters, v. 29, no. 7 [doi: 10.1029/2001GL013764].

Green, H. W., and Borch, R. S., 1989, A new molten salt cell for precision stress measurement at high pressure: European Journal of Mineralogy, v. 1, p. 213–219.

Green, H. W., and Burnley, P. C., 1989, A new self-organizing mechanism for deep-focus earthquakes: Nature, v. 341, p. 733–737.

Green, H. W., and Houston, H., 1995. The mechanics of deep earthquakes. Annual Review of Earth and Planetary Science, v. 23, p. 169–213.

Green, H. W., and Marone, C., 2002, Instability of deformation: Reviews of Mineralogy and Geochemistry, v. 51, p. 181–199.

Green, H. W., Young, T. E., Walker, D., and Scholz, C. H., 1990, Anticrack-associated faulting at very high-pressure in natural olivine: Nature, v. 348, p. 720–722.

Hacker, B. R., Peacock, S., Abers, G. A., and Holloway, S. D., 2003, Subduction factory 2. Are intermediate-depth earthquakes in subducting slabs linked to metamorphic dehydration reactions?: Journal of Geophysical Research, v. 108, B1 [doi: 1029/2001JB001129].

Jiao, W., Silver, P. G., Fei, Y., and Prewitt, C. T., 2000, Do intermediate- and deep-focus earthquakes occur on preexisting weak zones? An examination of the Tonga subduction zone: Journal of Geophysical Research, v. 105, p. 28,125–28,138.

Jin, Z-M., Green, H. W., and Zhou, Y., 1994, Melt topology in partially molten peridotite during ductile deformation: Nature, v. 372, p. 164–167.

Jung, H., Green, H. W., and Dobrzhinetskaya, L. F., 2004a, Intermediate-depth earthquake faulting by dehydration embrittlement with negative volume change: Nature, v. 428, p. 545–549.

Jung, H., and Karato, S., 2001a, Effects of water on dynamically recrystallized grain-size of olivine: Journal of Structural Geology, v. 23, p. 1337–1344.

Jung, H., and Karato, S., 2001b, Water-induced fabric transitions in olivine: Science, v. 293, p. 1460–1463.

Jung, H., Katayama, I., Jiang, Z., Hiraga, T., and Karato, S. 2004b, Effect of water and stress on the lattice preferred orientation (LPO) of olivine: Earth and and Planetary Science Letters, submitted.

Jung, H., and Waff, H. S., 1998, Olivine crystallographic control and anisotropic melt distributions in ultramafic

partial melts: Geophysical Research Letters, v. 25, p. 2901–2904.

Karato, S., 1995, Effects of water on seismic wave velocities in the upper mantle: Proceedings of the Japan Academy, v. 71, B(2), p. 61–66.

Karato, S., and Jung, H. 2003. Effects of pressure on high-temperature dislocation creep in olivine: Philosophical Magazine A, v. 83, No. 3, p. 401–414.

Karato, S., Paterson, M. S., and Fitz Gerald, J. D., 1986, Rheology of synthetic olivine aggregates: Influence of water and grain size: Journal of Geophysical Research, v. 91, p. 8151–8176.

Kasahara, J., Kamimura, A., Fujie, G., and Hino, R., 2001, Influence of water on earthquake generation along subduction zones: Bulletin of the Earthquake Research Institute, University of Tokyo, v. 76, p. 291–303.

Kayal, J. R., Zhao, D., Mishira, O. P., De, R., and Singh, O. P., 2002, The 2001 Bhuj earthquake: Tomographic evidence for fluids at the hypocenter and its implications for rupture nucleation: Geophysical Research Letters, v. 29, no. 24(5), p. 2152.

Kimball, K. L., Spear, F. S., and Dick, H. J. B., 1985, High-temperature alteration of abyssal ultramafics from the Islas Orcadas fracture zone. South Atlantic: Contributions to Mineralogy and Petrology, v. 91, p. 307–320.

Kirby, S., 1995, Intraslab earthquakes and phase changes in subducting lithosphere: Reviews of Geophysics, v. 33, supplement, p. 287–297.

Kodaira, S., Iidaka, T., Kato, A., Park, J-O., Iwasaki, T., and Kaneda, Y., 2004, High pore fluid pressure may cause silent slip in Nankai Trough: Science, v. 304, p. 1295–1298.

Kohlstedt, D. L., Kepler, H., and Rubie, D. C., 1996, Solubility of water in the α, β, and γ phases of $(Mg, Fe)_2SiO_4$: Contributions to Mineralogy and Petrology, v. 123, p. 345–357.

Maekawa, H., Yamamoto, K., Teruaki, I., Ueno, T., and Osada, Y., 2001, Serpentinite seamounts and hydrated mantle wedge in the Izu-Bonin and Mariana forearc regions: Bulletin of the Earthquake Research Institute, University of Tokyo, v. 76, p. 355–366.

Mackwell, S., Kohlstedt, D. L., and Paterson, M. S., 1985, Role of water in the deformation of olivine single crystals: Journal of Geophysical Research, v. 90, p. 11319–11333.

Meade, C., and Jeanloz, R., 1991, Deep-focus earthquakes and recycling of water into the Earth's mantle: Science, v. 252, p. 68–72.

Mei, S., and Kohlstedt, D. L., 2000, Influence of water on plastic deformation of olivine aggregates, 2. Dislocation creep regime: Journal of Geophysical Research, v. 105, p. 21,471–21,481.

Mishra, O. P., and Zhao, D., 2004, Seismic evidence for dehydration embrittlement of the subducting Pacific plate: Geophysical Research Letters, v. 31, L09610 [doi:10.1029/2004GL019489].

Murrell, S. A. F., and Ismail, I. A. H., 1976, The effect of decomposition of hydrous minerals on the mechanical properties of rocks at high pressures and temperatures: Tectonophysics, v. 31, p. 207–258.

Obara, K., 2002, Nonvolcanic deep tremor associated with subduction in southwest Japan: Science, v. 296, p. 1679–1681.

Omori, S., Kamiya, S., Maruyama, S., and Zhao, D., 2002, Morphology of the intraslab seismic zone and devolatilization phase equilibria of the subducting slab peridotite: Bulletin of the Earthquake Research Institute, University of Tokyo, v. 76, p. 455–478.

Ozawa, S., Hatanaka, Y., Kaidzu, M., Murakami, M., Imakiire, T., and Ishigaki, Y., 2004, Aseismic slip and low-frequency earthquakes in the Bungo channel, southwestern Japan: Geophysical Research Letters, v. 31, L07609 [doi:10.1029/2003GL019381].

Ozawa, S., Murakami, M., Kaidzu, M., Tada, Y., Sagiya, T., Hatanaka, Y., Yarai, H., and Nishimura, T., 2002, Detection and monitoring of ongoing aseismic slip in the Tokai region: Science, v. 298, p. 1009–1012.

Paterson, M., 1978, Experimental rock deformation—the brittle field, *in* Wyllie, P. J., ed., Minerals and Rocks: Berlin, Germany, Springer-Verlag, v. 13, p. 124–135.

Peacock, S., 2001, Are the lower planes of double seismic zones caused by serpentine dehydration in subducting oceanic mantle?: Geology, v. 29, p. 299–302.

Raleigh, C. B., 1967, Tectonic implications of serpentinite weakening: Geophysical Journal of the Royal Astronomical Society, v. 14, p. 45–51.

Raleigh, C. B., and Paterson, M. S., 1965, Experimental deformation of serpentinite and its tectonic implications: Journal of Geophysical Research, v. 70, p. 3965–3985.

Rispoli, R., 1981, Stress fields about strike-slip faults inferred from stylolites and tension gashes: Tectonophysics, v. 75, p. T29–T36.

Rogers, G., and Dragert, H., 2003, Episodic tremor and slip on the Cascadia subduction zone: The chatter of silent slip: Science, v. 300, p. 1942–1943.

Rutter, E. H., and Brodie, K. H., 1988, Experimental "syntectonic" dehydration of serpentinite under conditions of controlled pore water pressure: Journal of Geophysical Research, v. 93, p. 4907–4932.

Salah, M. K., and Zhao, D., 2003, 3-D seismic structure of Kii Peninsula in southwest Japan: Evidence for slab dehydration in the forearc: Tectonophysics, v. 364, p. 191–213.

Shan, Z., Stach, E. A., Wiezorek, J. M. K., Knapp, J. A., Follstaedt, D. M., and Mao, S. X. 2004, Grain boundary–mediated plasticity in nanocrystalline nickel: Science, v. 305, p. 654–657.

Seno, T., Zhao, D., Kobayashi, Y., and Nakamura, M., 2001, Dehydration of serpentinized slab mantle: Seis-

mic evidence from southwest Japan: Earth, Planets, and Space, v. 53, p. 861–871.

Silver, P. G., Beck, S. L., Wallace, T. C., Mead, C., Myers, S. C., James, D. E., and Kuehnel, R., 1995, Rupture characteristics of the deep Bolivian earthquake of 1994 and the mechanism of deep-focus earthquakes: Science, v. 268, p. 69–73.

Ulmer, P., and Trommsdorff, V., 1995, Serpentine stability to mantle depths and subduction related magmatism: Science, v. 268, p. 858–861.

Unsworth, M. J., Malin, P. E., Egbert, G. D., and Booker, J. R., 1997, Internal structure of the San Andreas fault at Parkfield, California: Geology, v. 25, p. 359–362.

Wang, K., Cassidy, J. F., Wada, I., and Smith, A. J., 2004, Effects of metamorphic crustal densification on earthquake size in warm slabs: Geophysical Research Letters, v. 31, L01605 [doi:10.1029/2003GL018644].

Wong, T. -F., Ko, S. C., and Olgaard, D. L., 1997, Generation and maintenance of pore pressure excess in a dehydrating system, 2. Theoretical analysis: Journal of Geophysical Research, v. 102, p. 841–852.

Zhang, H., Thurber, C. H., Shelly, D., Ide, S., Beroza, G. C., and Hasegawa, A., 2004, High-resolution subducting-slab structure beneath northern Honshu, Japan, revealed by double-difference tomography: Geology, v. 32, p. 361–364.

Zhang, J., Green, H. W., II, Bozhilov, K. N., and Jin, Z-M., 2004, Faulting induced by precipitation of water at grain boundaries in hot subducting oceanic crust: Nature, v. 428, p. 633–636.

Zhao, D., Kanamori, H., Negishi, H., and Wiens, D., 1996, Tomography of the source area of the 1995 Kobe earthquake: Evidence for fluids at the hypocenter?: Science, v. 274, p. 1891–1894.

Zhao, D., Mishra, O. P., and Sanda, R., 2002, Influence of fluids and magma on earthquakes: Seismological evidence: Physics of the Earth and Planetary Interiors, v. 132, p. 249–267.

Zhao, D., Tani, H., and Mishra, O. P., 2004, Crustal heterogeneity in the 2000 western Tottori earthquake region: Effect of fluids from slab dehydration: Physics of the Earth and Planetary Interiors, v. 145, p. 161–177.

Zimmerman, M. E., Zhang, S., Kohlstedt, D. L., and Karato, S., 1999, Melt distribution in mantle rocks deformed in shear: Geophysical Research Letters, v. 26, p. 1505–1508.